Influence of microstructure on the dynamic behavior of a polyurethane foam with the material point method

Nicolas Lelong, Denis Rochais

Version of Record: https://www.sciencedirect.com/science/article/pii/S2589152918302394
Manuscript_e2624c71dcb2bfd3dd835316cd12730c

Influence of microstructure on the dynamic behavior of a Polyurethane foam with the Material Point Method

Nicolas Lelong, Denis Rochais

CEA, DAM, Le Ripault, BP16, 37260 Monts, France.

Abstract

Polymer foams have many industrial applications because of their good mechanical properties combined with low material density. However, their study and the prediction of their behavior is challenging due to the massive influence of their complex microstructure. This paper focused on a polyurethane foam containing 70 vol% of porosity and aims at determining its behavior when submitted to large deformations under dynamic compressive loads. A model based on the material point method was set to study the whole stress-strain relationship of representative realistic foam sample, obtained from CT-scans. The dynamic model was validated to compression results from Split Hopkinson Pressure Bar experiments allowing the study of a shock due to a container fall. Direct influence of the microstructure was then evaluated. We first added virtual realistic manufacturing defects on the geometry and then studied the foam behavior of fully computer-designed microstructures. Recent developments in additive fabrication make the manufacturing of such structures possible and would widen the possibilities of virtually optimizing material designs.

1 Introduction

Polyurethane foams are massively used for a wide range of applications in engineering, because of their relatively high strength, good thermal or acoustic properties, combined with low cost and low density. Such materials are especially designed to absorb handling shock energy or mechanical loads. Engineering applications of cellular materials are perpetually

increasing, making the optimization of their design an important matter for industrials. The behavior of foams under different mechanical loads at various rates has to be investigated. But the macroscopic response of such materials is directly related to the complex microstructure of the material [1, 2]. Many experimental studies helped determine some correlations between microstructure and bulk behavior [2, 3, 4] but also showed the necessity to include the microstructure geometry for analyzing the mechanical behavior of the foam. Furthermore, in the case of polymer foams, the foaming process can affect bulk material mechanical properties [5].

There are many types of microstructures, with either isolated or connected pores, depending on the manufacturing process. For example, materials like polyurethane foams are made of randomly scattered spherical gas bubbles in a polyurethane matrix. The dynamics of compression is then three-dimensional at the microscopic scale, at the scale of the solid pores membrane [6]. This kind of foam is typically used to resist compression so only this type of load is considered in this study. Its purpose is then to determine the bulk behavior of the foam by accounting the specifics of the complex microstructural geometry of the material. The macroscopic stress-strain response of a porous material under compression has three typical phases (figure 1) [7]. First the stress increases linearly with the strain at small deformations, characterized by the Young's modulus. When a yield stress is reached begins a plateau with a hardening slope. Then the densification phase begins when approaching a bulk behavior. [8] These characteristics depend mainly on the microstructure, whose modelling remains the main challenge. Numerical modeling has been considered and while the potential gain in understanding the relationship between geometry and material response, it also raised some important challenges, especially to describe with enough accuracy the complex microstructure of actual foams.

Some models already exist for microstructures with regular pores. For example, the model of Gibson and Ashby [7] or Kelvin cells [9, 10] can be used to describe the geometric structure of a foam with regularly shaped pores. But these approaches are mostly restricted to low density foams. Other methods have been developed to describe numerically the geometry of irregular and anisotropic microstructures, such as Voronoi tessellation [1, 11].

Finally, the actual foam microstructure can be directly obtained through X-ray tomography with increasing quality and resolution. The finite element method (FEM), widely used in solid mechanics, has been already successfully applied for quasi-static cases of foam compression [12]. FEM requires the solid part of the structure to be discretized for creating the mesh, which could be difficult with such geometries [13]. FEM-based simulation studies on CT microstructures are limited to small deformations and the beginning of the stress-strain plot [12, 14, 15]. When the foam densifies, interactions between collapsing pore walls cannot be managed. These models are able to get the elastic response but fail to handle large deformations and multiple contacts between the pores. Furthermore, when the foam is applied moderate macroscopic deformations, it implies large deformations, rotations and material contacts at the microscopic scale. Densification is caused by the collapse of the microstructure. To include contacts, typical FEM algorithms need to specify where these contacts would occur, which becomes impossible when deformation increases.

Particle models and especially particle-in-cell methods are particularly suited for this kind of issue. Bardenhagen [16] showed the relevance of using the material point method (MPM) for compressing a foam microstructure. The stress-strain relation has been obtained on the whole deformation range, until the densification phase. It also showed the strong link between the microstructure and the macroscopic response of the material.

This paper presents a numerical model simulating the dynamic compression of polyurethane foam. Results were compared to experimental results previously obtained with the split Hopkinson pressure bar (SHPB) method. After validation, influence of the microstructure on the mechanical behavior of the foam was studied. At first, artificial larger cavities were included in the foam to test the modified stress-strain curve. Then virtual structures were designed to determine the geometric structures leading to a given behavior. Performance of MPM on foam compression cases could be evaluated.

2 Methods

2.1 Material Point Method

The Material Point Method finds its origin in particle-in-cell methods, where particles, referred as material points, were used to carry the state variables of the material and handle its deformation [17]. It has been first introduced by Sulsky [18] as an alternative for solid mechanics cases. This method showed good accuracy and robustness to handle material contacts [16]. Then Bardenhagen and Kober [19] developed the generalized interpolation material point method (GIMP), a general mathematical framework from which MPM could be derived, offering similar accuracy as finite elements methods and capable to handle large deformations.

MPM is basically an Arbitrary Lagrangian-Eulerian (ALE) method, Lagrangian particles moving through an Eulerian mesh. In GIMP, every material body is described as particles, which contains material properties and current state variables (stress, strain, velocity…). Particle mass is constant, so mass conservation is implicitly validated. A fixed regular background grid is used. Variables are interpolated on that grid and Lagrangian momentum equations are solved. Positions and velocities of particles could then be updated [20]. The background grid keeps no state information and can be reset at each time step, thus preventing

mesh entanglement, which occurs in case of large deformations. Details on the method can be found in [21]. The use of particles to carry material variables allows the tracking of material interfaces and then solving contacts between surfaces.

More recently, another improvement was added to the GIMP framework, the convective particle domain interpolation [22]. The deformation tensor obtained by solving the momentum equations is also applied on the particle shape function. This method showed better performances for the handling of very large rotations and deformations, but with a higher computational cost.

All MPM calculations presented in this paper were run with the University of Utah C-SAFE code, named Uintah. It showed good parallel performances on foam compaction cases [5]. It was especially chosen to perform these calculations because it could directly handle CT scans as raw images. Voxels are directly taken as material particles and no meshing is necessary. Furthermore, Uintah is flexible and enables adding customized constitutive laws.

2.2 Polyurethane Foam

2.2.1 Geometry

This paper analyzes the characterization of a polyurethane (PUR) foam with a density d = 316 kg/m^3. Its 3D microstructure has been observed through CT scans, with a resolution going down to 1.62 µm/voxel. These scans were carried out at the European Synchrotron Research Facility in Grenoble, France. The observed microstructure showed interpenetrating spherical pores, separated by thin PUR walls.

CT raw images had low contrast between the PUR walls and the void phase. Images obtained after simple thresholding analysis were noisy. The images were then analyzed by Markov segmentation [23] to get accurate contours of the cavities. The segmented image is shown on

figure 2. PUR voxels were set to a value of 1 and air voxels set to 0. PUR volume fraction was computed at 29.4 %.

2.2.2 Mechanical properties

In order to compute the behavior of the foam under compression, mechanical characteristics of solid skeleton PUR are needed. Then, "Bulk" polyurethane samples were produced without adding water. Mechanical properties of this bulk PUR are then assumed to characterize the local behavior of the edges and faces of the foam pores. Compressive behavior of bulk PUR is however not completely representative of the local behavior of the skeleton which is then subject to various loads (traction, compression or shear). We then chose to use the flexural behavior of the bulk PUR to model the solid part of the foam, since a flexural load usually combines traction and compression.

$$\sigma = \begin{cases} E\varepsilon & \sigma \leq \sigma_y \\ \sigma_y + E_h(\varepsilon - \varepsilon_y) & \sigma_y \leq \sigma \leq \sigma_f \\ 0 & \sigma_f \leq \sigma \end{cases} \quad \text{(Eq. 1)}$$

A 4-point bending test on that material provided a stress-strain curve, which could be injected in Uintah. Then the constitutive model was taken as an elastic-plastic bilinear law with damage, described by equation 1, with σ the Cauchy stress and ε the deformation, using following constant values: Flexural Young's modulus E = 2.76 GPa, Poisson's ratio ν = 0.33, Flexural yield stress σ_y = 68.4 MPa (with corresponding yield deformation $\varepsilon_y = \sigma_y/E$), hardening modulus E_h = 1.34 GPa, critical stress σ_f = 127 MPa.

2.3 Experimental setup – Hopkinson

Compression experiments were conducted with the Split Hopkinson Pressure Bar (SHPB) method. This method consists in placing the sample between two long cylindrical bars (the incident bar and the transmission bar). Then a striker bar, usually launched by compressed

gas, impacts the incident bar and generates an elastic incident wave, which propagates through the sample and the transmission bar (figure 3). Incident and transmitted signals are recorded through strain gages placed on the bars [24]. This experimental set-up allows reproducing shock induced by a container fall for instance. Because of the low impedance of the PUR foam, 7075-T6 Aluminum bars with a 20 mm diameter were used [24]. With aluminum, the transmitted pulse has higher amplitude than with steel, which is conventionally used for SHPB but is not applicable for soft materials like foams [25]. Within the load range, the behavior of aluminum stays elastic. Incident and transmitter bars are respectively 2.5 and 2 m long, whereas the striker bar is 1.05 m long. The link between the bars and the foam sample is carried out by two 7075-T6 Aluminum movable pistons, adapted to the diameter of the sample. Then a 35NCD16 Steel 5-mm-thick and 10-mm-long hollow cylinder is used to confine the sample laterally. Incident and transmitter bars are equipped with strain gages placed at 1.25 m from the incident piston and 0.30 m from the transmitter piston. Gages are powered with Vishay 2230B signal conditioners and tension variations are recorded with a Lecroy digital recorder, from which strain can be obtained. Data analysis is provided by software DAVID. Because of the elastic behavior of the aluminum, determination of stress applied on the foam is straightforward. Dynamic stress equilibrium must be controlled in order to validate the results [26]. This was ensured by checking that the transmitted signal corresponded to the difference between the incident and the reflected signal. Each of these signals is provided in DAVID.

10 foam samples were tested through this method, each one originating from the same manufacturing batch. Foam samples are cut as 10 mm diameter cylinders with a 2 mm thickness. In order to set the numerical model, the velocity of the incident bar was recorded.

2.4 Numerical model

2.4.1 Piston velocity

The numerical model reproduces the experimental conditions of the SHPB setup. Input is characterized by the strain rate, hence the velocity, of the incident bar. The velocity pulse is recorded by the incident bar strain gage. Maximal amplitude recorded was about 7 m/s, corresponding to a strain rate of 3000 s^{-1}.

Compression of the foam was simulated through a rigid piston moving along the z-axis. Setting a constant velocity profile at the value would cause acceleration effects at the beginning of the compression, as the piston hits the foam. Thus the velocity of the foam was set to replicate the exact velocity profile recorded by the Hopkinson bar, enabling a smoother initial stress gradient.

2.4.2 Setting the model

One of the main advantages of MPM is the simplicity of mesh design. The 3D raw images obtained from the CT scans are used as direct geometry input for Uintah computations. Raw images contained up to 1500 voxels in each direction, then samples were cut according to simulation needs. A points file is produced with the list of cartesian coordinates of the center of voxels containing the material. Each of these voxels and points matches a material particle, as defined in MPM. The Eulerian mesh is set so that each cell contains two particles in each direction. That repartition is suggested to optimize accuracy and computation time [19]. The piston is a thin (10 particles or 50 µm) square plate with infinite stiffness moving along the z-axis. Boundary conditions are defined as periodic for the x and y directions. The diameter of the pores (mostly smaller than 100 µm) is much smaller than the dimensions in those directions and their repartition is random, so, at the scale of the sample, periodicity is a reasonable assumption.

The motion of the piston is controlled by a velocity profile matching the Hopkinson bar setup. The time step is dynamically computed to handle properly the propagation of the compression longitudinal wave. To ensure stability, particle motion at each time step should not be larger than its size. So the time step is defined by $\Delta t = \frac{\Delta x}{\max(v_p,u)}$, where v_p is the piston velocity, $u = \sqrt{\frac{E+2\mu}{\rho}}$ the wave propagation velocity, and Δx the particle size. Boundary conditions are defined as periodic for the x and y directions. Theoretical wave velocity is about 1300 m/s whereas maximal piston velocity is 6 m/s. So the time step is lower than 4 ns. A large number of time steps are then necessary to compute a reasonable amount of physical time. To run each case until the foam reached a quasi-dense state, around 70 % strain, about 0.2 ms would be needed. Piston velocity being much lower than wave velocity, this ensures that dynamic effects bound to wave propagation stays negligible. Density of bulk PUR was measured on experimental samples at 1040 kg/m³. As described in [22], a more precise interpolation scheme could be used : the Convected Particle Domain Interpolation (CPDI) which was found to be relevant on very large local deformations. This scheme was tested with Uintah on some samples and it was shown that in our foam compaction cases, CPDI is three times more time consuming for negligible increase of accuracy.

As stated before, the PUR skeleton is described by an elastic-plastic stress-strain law. The yield condition uses the von Mises stress. This “equivalent stress” is a norm of the stress tensor, defined by $\sigma_{eq} = \sqrt{\frac{3}{2}\sum_{ij}\sigma'_{ij}\sigma'_{ij}}$, where σ' is the stress deviator. This stress summarizes the contribution of each type of mechanical load: compression/traction, flexion and shear. Indeed, even if the main load is compression, we could consider that these phenomena would occur at a microscopic scale on foam “strings”. Therefore, to get a macroscopic response of the material under compression, an equivalent stress would be relevant.

Stress is set to be recorded by Uintah at each time step at the bottom face of the foam, opposite to the piston. Strain rate is computed at each time step with the instant piston velocity, linearly interpolated from the injected Hopkinson velocity profile. Then the stress-strain law of the foam could be plotted. Uintah results are visualized through the VisIt software allowing the display of the evolution of the particle stresses during the compression.

In parallel computing with Uintah, the grid is divided into parallelepiped domains, each of them handled by a processor. In our case the repartition of the pores in the foam being random, each domain would contain a similar amount of particles. So the load is evenly spread among processors. Each processor deals with its own set of particles, solves equations, and writes resulting data files. MPM cases were run on the CCRT facility (Centre de Calcul pour la Recherche Technologique, Bruyères-le-Châtel, France). This supercomputer provides a performance of 420 Teraflops over 9500 available computing cores. After some scalability tests on smaller foam samples, the case showed good parallel performance and Uintah was optimized to be run on up to 1024 processors.

2.4.3 Redesigning the microstructure

This paper aims at demonstrating the important influence the microstructure would have on the mechanical response of the foam. For this purpose, we need to compute the behavior of various types of structures. We first modified the structure of the original PUR foam by introducing spherical or ellipsoidal cavities, representing realistic faults that could be created in the manufacturing. Then, in order to determine the direct influence of the geometry on the bulk mechanical properties, structures have been numerically designed as raw images with periodic voxelized patterns. Each pattern was made out of usual volumes: spheres, cylinders, ellipsoids, parallelepipeds… used as blocks or cavities. A numerical tool was designed to create or modify three-dimensional raw image files by designing voxelized simple shapes that could be easily added to or subtracted from each other or from real CT-scanned foam.

The amount of structures to be tested in order to perform an exhaustive parametric study would be huge because it implies a large quantity of settable parameters: type and size of the shapes, orientation and layout of patterns, density, mixing layers of different patterns. The material skeleton used was PUR, with the same mechanical properties as described before. We also chose to design the structures with a similar solid volume fraction, around 30 %, to ensure a proper comparison between the patterns. Furthermore, every sample was cut at 400^3 voxels, this being a compromise for the volume to be representative and to be computed in reasonable time with Uintah.

3 Results

3.1 Uintah vs. Experiments

Stress strain plots matching the dynamic compressive behavior obtained with SHPB experiments on 10 samples give a hint about the variability of such material and the measurement method. Regarding the elastic phase, the mean Young's modulus is 310 MPa, with a range from 240 to 350 MPa, corresponding to about ±20% deviation.

CT scans of the PUR foam have a resolution of 5 µm/voxel. Experimental samples analyzed with Hopkinson bars are 2 mm thick, so a 400x400x400 voxel image was chosen as a maximal representative volume. However, since a Uintah computation with such a large file is time-consuming, smaller samples were cut inside that image for preliminary tests. Samples with 100x100x100 and 200x200x200 voxels were then also generated. Figure 4 shows the results comparing these samples. This figure indicates that the overall profile of the stress-strain behavior seems converging to the 400^3 sample and we can assume that a larger sample will not give access to different phenomena. Plots corresponding to 200^3 voxels and 400^3 voxels show no major differences between each other.

Figure 5 compares the stress-strain plots obtained experimentally with SHPB and numerically with Uintah. The experimental plot corresponds to the mean on the tested samples. Both cases show a similar profile. First the foam has an elastic behavior characterized by a Young's modulus around 300 MPa. Then the stress reaches a plateau at 15 MPa. It slightly increases in the numerical plot when the experimental plot is stable. Finally, in both cases, at around 50 % strain, the foam begins its densification. The dynamics of the compression of the PUR foam can be numerically obtained at a high strain rate (~ 3000 s^{-1}) over the whole strain range.

3.2 Geometry alterations

During the manufacturing of the foam, especially in the foaming phase, larger cavities (up to 1 mm diameter) could form due to irregularities in the material. This phenomenon modifies the microstructure, thus potentially altering the mechanical behavior of the foam. To analyze that, spherical or ellipsoidal pores, larger than actual bubbles, were added inside the foam. Those kinds of pores could be observed on actual manufactured foam. Pores with different sizes, orientations and positions were tested, matching realistic manufacturing defects. The base geometry used here was a 200x200x300 voxel PUR foam volume, the 300 voxels being along the z-axis, which is the direction of compression. The whole sample was not necessary for these computations, given the fact that a relative variation from the base foam stress-strain curve was to be observed.

The purpose of the first set of tested defects is to determine for a given missing volume what configuration alters the most the mechanical response, if defects are single or multiple. It compared a foam sample with a larger spherical pore in its center to one with two identical pores with half volume, so that the solid volume fraction doesn't change. In the first case, the original pore is a sphere with 0.5 mm diameter, divided into two spheres with 0.4 mm diameter. Stress-strain plots on figure 6 indicate that there is no significant change between

these two configurations. However, when a larger cavity is included (0.8 mm diameter vs. two 0.64 mm spheres), the yield stress drop is slightly more important with two spheres. At higher strain, the stress profile is identical for the same volume fraction.

Ellipsoidal cavities were then compared in order to analyze the influence of position and orientation of the defect. The volume of the added ellipsoids, all with the same volume, represents less than 2 % of the overall foam volume (1.5 mm^3). In the following, the direction of compression of the piston is set as the z-axis. Both other axes x and y are taken arbitrarily perpendicular to the direction of compression. The first configuration introduces an ellipsoid whose major axis is along x axis and is twice as large as the other axes. The two other configurations introduce a more eccentric ellipsoid, whose two major axes are 8 times larger than the minor one. First one is thinner along y whereas the other one is thinner along z. In each case, the added cavity is set at the center of the sample. Tests with ellipsoidal cavities set at the top or the bottom of the structure demonstrated that this setting does not influence the macroscopic response. Figure 7 show results obtained with these configurations. The plot indicates that, for an ellipsoid larger along z, the influence of the altered geometry is low, especially for the elastic phase. On the other hand, an ellipsoid defect, larger along x and y, would introduce a much lower solid fraction locally in the xy cross-section at the defect positionand cause a drop of the yield stress. However, in these cases, the plastic plateau stays at a similar level as the base sample.

3.3 Virtual structures

In this paper, we computed two series of structures. The first cases considered porous foams, as depicted on figure 8. These structures are formed by a solid block hollowed out by spherical or ellipsoidal pores with identical dimensions. Each structure is periodic along the three axes and has a volume fraction around 30 %.

The results are depicted on figure 9. These plots show the stress-strain curves obtained with spherical pores (a) or ellipsoidal pores with high eccentricity, whose major axis oriented in the direction of compression (b) or perpendicular to it (c). Figure 9 show large differences between these structures in terms of mechanical behavior, especially the structure with vertical ellipsoids (c). After reaching the yield stress, around 3 % strain, the stress on structure c decreases, oscillates and reach a plateau around 5 MPa, where stress on structure b keeps increasing to stabilize later around 50 MPa. Finally, all these curves have similar profile in the densification phase, when the influence of the microstructure is lower. Only the critical strain, which is directly related to the volume fraction, differs with the microstructure. These results show how a microstructure can alter significantly the foam behavior during compression. The mixed ellipsoids layout (d), which consisted of successive layers of vertical and horizontal ellipsoids, shows an averaged behavior. Until about 30 % strain, its behavior is similar to configuration (b) but its densification phase is similar to configuration c. By using different layers of various patterns, a material with a desired behavior could be designed.

The second set of structures, displayed on figure 10, used bars with differently shaped sections and different layouts. The dimensions of the bars are computed in such a way that the volume fraction is conserved. The “crossed” pattern consists of bars aligned along the diagonals of the faces of a cube, corresponding to the base cell of the structure (a). 3 versions of this structure were made, the bars having a square, round or elliptic section, with in each case the same section area. The elliptic one has a major axis twice as large as its minor axis. In diamond structure, bars link the nodes matching the position of carbon atoms in a diamond crystal pattern (b). Kelvin cells configuration is designed with bars set along the edges of a tetrakaidecahedron (c), a structure often encountered in foam studies. Base cells are set at 50^3 voxels, 100^3 for the Kelvin cells, and the computed sample has 6 (3 for Kelvin) cells in each direction, so contains 300^3 voxels. Samples are then fully periodic in every dimension. For

each of these structures, the size of the bars, all identical, has been determined in order to match approximately 30 % volume fraction. Figure 11 show the plots obtained with these structures. No major differences can be observed between round and square bars, but elliptic ones increase significantly the Young's modulus, yield stress and plastic plateau. With a Kelvin cell structure, no actual stress plateau is observed during the plasticity phase. Stress is monotonously increasing in that phase. Diamond structure implies a peculiar behavior: The Young's modulus is twice as high as the crossed configuration, as well as the plastic plateau, at 20 MPa. However, this plateau stays constant until reaching 60 % strain. As previous results also showed, densification is not influenced by the microstructure but depends only on overall volume fraction. In summary, these configurations illustrate the major influence the shape and the layout of solid bars in a foam could make on its behavior, regardless of its base material.

4 Discussion

4.1 Dynamic foam compression

Results presented in this paper showed that the mechanical behavior of relatively dense (28 % volume fraction) polymer foam can be numerically obtained through MPM over the whole strain range. Uintah was able to reproduce the dynamic compression of a PUR foam sample by the SHPB method. The three phases of the stress-strain relationship (elastic phase, plastic phase and densification) have been obtained. Young's modulus, yield stress and critical strain (beginning of densification) are matching within an acceptable range. The manufacturing process of polymer foams such as PUR foams lead to a microstructure with randomly scattered pores. The pore repartition induces significant variations in the characteristics of their dynamic compressive behavior. Hopkinson experiments showed that the measured

Young’s modulus can range from about 20 % around its mean value inside the same manufacturing batch. Yield stress range from 12.5 to 15.1 MPa, also 20 % variation.

MPM computations provided a macroscopic response to a compressive load on the material. The actual geometry of the sample was accounted at a microscopic scale. However, the mechanical properties and the constitutive law representative of skeleton foam are not precisely known. A behavior approximation on densified PUR samples had to be done. Furthermore, at the scale of one string of PUR skeleton, the material is subject to various kinds of loads: not only compression but also traction, bending or shear. Experimental tests could not be performed easily to characterize these loads. That's why the sample volume needs to average the microscopic loads in order to get the macroscopic response. The 400^3 sampled volume used to model the foam was found to be representative enough to provide a reliable macroscopic structure. A larger mesh size would strongly increase computation time without offering significantly better accuracy of the model. An other improvement possibility would be refining the mesh using for example CT scans with a better resolution, but then, to be representative, image size (in voxels) would have to be increased, as well as the computation time.

In order to assess how the microstructure influences the stress-strain law of a foam, independently of its mechanical properties, altered microstructures were numerically computed with Uintah. After slightly altering the foam in terms of solid volume loss, virtually introducing defects inside the regular pores, the dynamic response could be significantly modified. The size of the defects (large spherical or ellipsoidal pores) is typical of encountered manufacturing defects. On the stress-strain plots, the observed losses in terms of yield stress increase in relation to the section area of the defect in the plane normal to the direction of compression. However, the Young's modulus and the level of the stress plateau during the plasticity phase are rather dependent of the resulting volume fraction. Tests with

ellipsoidal defects showed that a low volume fraction loss (~ 2%), depending on its shape, can significantly reduce the stiffness of a material, therefore its effectiveness regarding load absorption. These results emphasize the relevance of manufacturing foam materials with a numerically designed microstructure through 3D printing.

4.2 Optimization through virtual microstructures

MPM offered a reliable numerical model to characterize a polymer foam microstructure for dynamic compression. Results obtained with virtual microstructures confirm the importance of a numerical microstructural analysis of foam materials and the determination of an effective manufacturing process. Nowadays, additive manufacturing (AM) has become a massively used technique in many fields, like jewelry or medical prosthetics. It provides good accuracy and reproducibility, and avoids material losses. For complex structures with high resolution, 3D printing may be the fastest and cheapest manufacturing process [27]. It also enables new designs, setting new assemblies with custom mechanical properties. Therefore, the crafting and even manufacturing of artificially designed foams through AM become conceivable. It opens a new field of material structures, whose mechanical behavior could be numerically computed and then determined before production, reducing design time and costs. Much less or even no alteration during the manufacturing process would occur, causing the behavior of the whole material to be invalid. The deformation behavior of the material could be known at a microstructural scale. It would then offer a whole new range of optimization opportunities to design a foam with a customized stress-strain relationship. For example, shock absorbing materials would generally need a high stiffness coupled with low solid volume fraction, implying a late densification.

However, the parametric study to determine the mechanical behavior of a particular microstructure contains a large quantity of settable parameters: type and size of the shapes,

orientation and layout of patterns, density, mixing layers of different patterns. Geometries shown in this paper are just a glimpse into microstructure possibilities and an exhaustive parametric study would need a lot of computation time. While MPM demonstrated its capabilities for characterization of foam materials, its relatively high computation time (about 24 hours for a 400^3 voxels structure) makes it difficult for browsing a large range of designs. Yet computation time can be reduced by using geometries constructed on periodic base cells.

Results obtained with PUR foam showed that, with a representative volume, loads applied at a microstructural scale were averaged on the macroscopic response. With the same material properties, changing the microstructure lead to highlight different behaviors. By widening the investigation range, we would necessarily move forward into the customization of an optimized foam material. For a given desired set of mechanical properties, literature can also provide hints for designing the microstructure. Many studies focused on designing materials with prescribed mechanical properties, even before the rise of AM. For example, structures having extreme elastic properties were presented [28]. Guest and Prevost [29] showed structures maximizing bulk modulus and permeability. Panetta et al. [27] browsed various structures and characterized their elastic properties, both from simulation and from experiments on 3D-printed samples. However these studies are mostly restricted on the elastic phase and relate to a few static parameters. Our paper showed that a similar investigation can be made about the dynamic behavior of foams and with MPM, we are able to get the whole behavior. The numerical model did not include any PUR- or polymer-related property. Numerical results could be correlated to experimental data using an isotropic elastic-plastic constitutive model. This suggests that the observed behavior would not be much influenced by the nature of the bulk material. This study can be used as basis for an exhaustive parametric study of structures providing given macroscopic responses.

Such structures can now be considered for actual materials. Before using them, it is however necessary to validate experimentally the analytically or numerically computed properties, which is now possible through AM. Future work would first need to establish correlation between numerically computed dynamic behavior of a numerically designed microstructure and the measured behavior of a 3D-printed sample, over the whole strain range.

Conclusion

Material point method was proven effective to compute the mechanical behavior of PUR foam at a dynamic strain rate. Numerical results have been validated over the whole strain range in relation to experimental data obtained with the SHPB method. MPM was able to account for the complex geometry of PUR foam (70 vol% of porosity) in order to get its macroscopic response, when submitted to a compressive load. This model could then be used to evaluate the direct influence of the microstructure over the bulk material properties. Tests with additional cavities inside the structures, representing realistic manufacturing defects, showed how little volume loss could massively disrupt the nominal behavior of the foam. This illustrates the need for a more reliable manufacturing process for load-absorbing materials, like additive manufacturing, which is now available. Preliminary computations were made with MPM on customized periodic structures and show the potential of an exhaustive parametric study for designing an optimized foam material for a desired mechanical behavior.

References

[1] H. Zhu and A. Windle, "Effects of cell irregularity on the elastic properties of open-cell foams," *Acta Materialia*, vol. 50, pp. 1041-52, 2002.

[2] L. Gong, S. Kyriakides and W. Jang, "Compressive response of open-cell foams. Part I: Morphology and elastic properties," *Internatinal journal of solid structures*, vol. 45, pp. 1355-79, 2005.

[3] H. Zhu, J. Knott and N. Mills, "Analyses of the elastic properties open-cell foams with tetrakaidecahedral cells," *Journal of the mechanics and physics of solids,* vol. 45, pp. 319-43, 1997.

[4] J. Elliott and A. Windle, "In-situ deformation of an open-cell flexible polyurethane foam characterised by 3D computed microtomography," *Journal of Material Science,* vol. 37, pp. 1547-55, 2002.

[5] A. Brydon, S. Bardenhagen, E. Miller and G. Seidler, "Simulation of the densification of real open-celled foam microstructures," *Journal of the Mechanics and Physics of Solids,* vol. 53, pp. 2638-60, 2005.

[6] F. Saint-Michel, L. Chazeau, J. Cavaillé and E. Chabert, "Mechanical properties of high density polyurethane foams : I. Effect of the density," *Composites Science and Technology,* vol. 66, pp. 2700-8, 2006.

[7] L. Gibson and M. Ashby, Cellular Solids: Structure and Properties, 2nd ed., Cambridge, MA: Cambridge University Press, 1997.

[8] P. Tan, S. Reid and J. Harrigan, "On the dynamic mechanical properties of open-cell metal foams - A re-assesment of the 'simple-shock theory'," *International Journal of Solids and Structures,* vol. 49, pp. 2744-2753, 2012.

[9] W. Warren and A. Kraynik, "Linear elastic behavior of a low density Kelvin foam with open cells," *Journal of applied mechanics,* pp. 787-94, 1997.

[10] N. Mills, R. Stämpfli, F. Marone and P. Brühwiler, "Finite element micromechanics model of impact compression of closed-cell polymer foams," *International Journal of Solid Structures,* vol. 46, pp. 677-97, 2009.

[11] C. Barbier, P. Michaud, D. Baillis, J. Randrianalisoa and A. Combescure, "New laws for the tension compression properties of Voronoi closed-cell polymer foams in relation to their microstructure," *European Journal of Mechanics and Solids,* vol. 45, pp. 110-22, 2014.

[12] S. Youssef, E. Maire and R. Gaertner, "Finite element modeling of the actual structure of cellular materials determined by X-ray tomography," *Acta Materialia,* pp. 719-730, 2005.

[13] G. Seidler, L. Atkins, E. Behne, U. Noomnarm, S. Koehler, R. Gustafson and W. McKean, "Application of synchrotron X-ray microtomography to mesoscale materials," *Advanced Complex Systems,* vol. 4, pp. 481-90, 2001.

[14] V. Shulmeister, M. Van der Burg, E. Van der Giessen and R. Marissen, "A numerical study of large deformations of low-density elastomeric open-cell foams," *Mechanics of*

Materials, vol. 30, pp. 125-40, 1998.

[15] S. Vajjhala, A. Kraynik and L. Gibson, "A cellular solid model for modulus reduction due to resorption of trabeculae in bone," *Journal of biomechanical engineering,* vol. 122, pp. 511-5, 2000.

[16] S. Bardenhagen, A. Brydon and J. Guilkey, "Insight into the physics of foam densification via numerial simulation," *Journal of the mechanics and physics of solids,* vol. 53, pp. 597-617, 2005.

[17] J. Brackbill, D. Kothe and H. Ruppel, "FLIP: a low-dissipation, particle-in-cell method for fluid flow," *Journal of Computational Physics,* vol. 48, pp. 25-38, 1988.

[18] D. Sulsky and S. S. H. Zhou, "Application of a particle-in-cell method to solid mechanics," *Comput. Phys. Commun.,* no. 87, pp. 236-52, 1995.

[19] S. Bardenhagen and E. Kober, "The generalized interpolation material point method," *Computational Models for Engineering Science,* vol. 5, pp. 477-95, 2004.

[20] J. Burghardt, R. Brannon and J. Guilkey, "A non local plasticity for the material point method," *Computational Methods Applied to Mechanical Engineering,* Vols. 225-8, pp. 55-64, 2012.

[21] M. Steffen, P. Wallstedt, J. Guilkey, R. Kirby and M. Berzins, "Examination and analysis of implementation choices within the material point method," *Computational Modelling in Engineering Science,* vol. 31, pp. 107-127, 2008.

[22] A. Sadeghirad, R. Brannon and J. Burghardt, "A convected particle domain interpolation technique to extend applicability of the material point method for problems involving massive deformations," *International Journal for Numerical Methods in Engineering,* vol. 86, pp. 1435-56, 2011.

[23] S. Li, Markov random field modeling in image analysis, London: Springer-Verlag, 2009.

[24] B. Song and W. Chen, "Split Hopkinson pressure bar techniques for characterizing soft materials," *Latin American Journal of Solids and Structures,* pp. 113-152, 2005.

[25] W. Chen, B. Zhang and M. Forrestal, "A split Hopkinson pressure bar technique for low impedance materials," *Experimental Mechanics,* vol. 39, pp. 81-85, 1999.

[26] W. Chen, F. Lu and N. Winfree, "High-strain-rate compressive behavior of a rigif polyurethane foam with various densities," *Experimental Mechanics,* pp. 65-73, 2001.

[27] J. Panetta, Q. Zhou, L. Malomo, N. Pietroni, P. Cignoni and D. Zorin, "Elastic textures for additive fabrication," *ACM Transactions on Graphics,* vol. 34, no. 135, pp. 1-12,

2015.

[28] O. Sigmund, "Tailoring materials with prescribed elastic properties," *Mechanics of Materials,* vol. 20, pp. 351-68, 1995.

[29] J. Guest and J. Prevost, "Optimizing multifunctional materials: design of microstructures for maximized stiffness and fluid permeability," *International Journal of Solids and Structures,* vol. 2223, pp. 7028-47, 2006.

List of figures

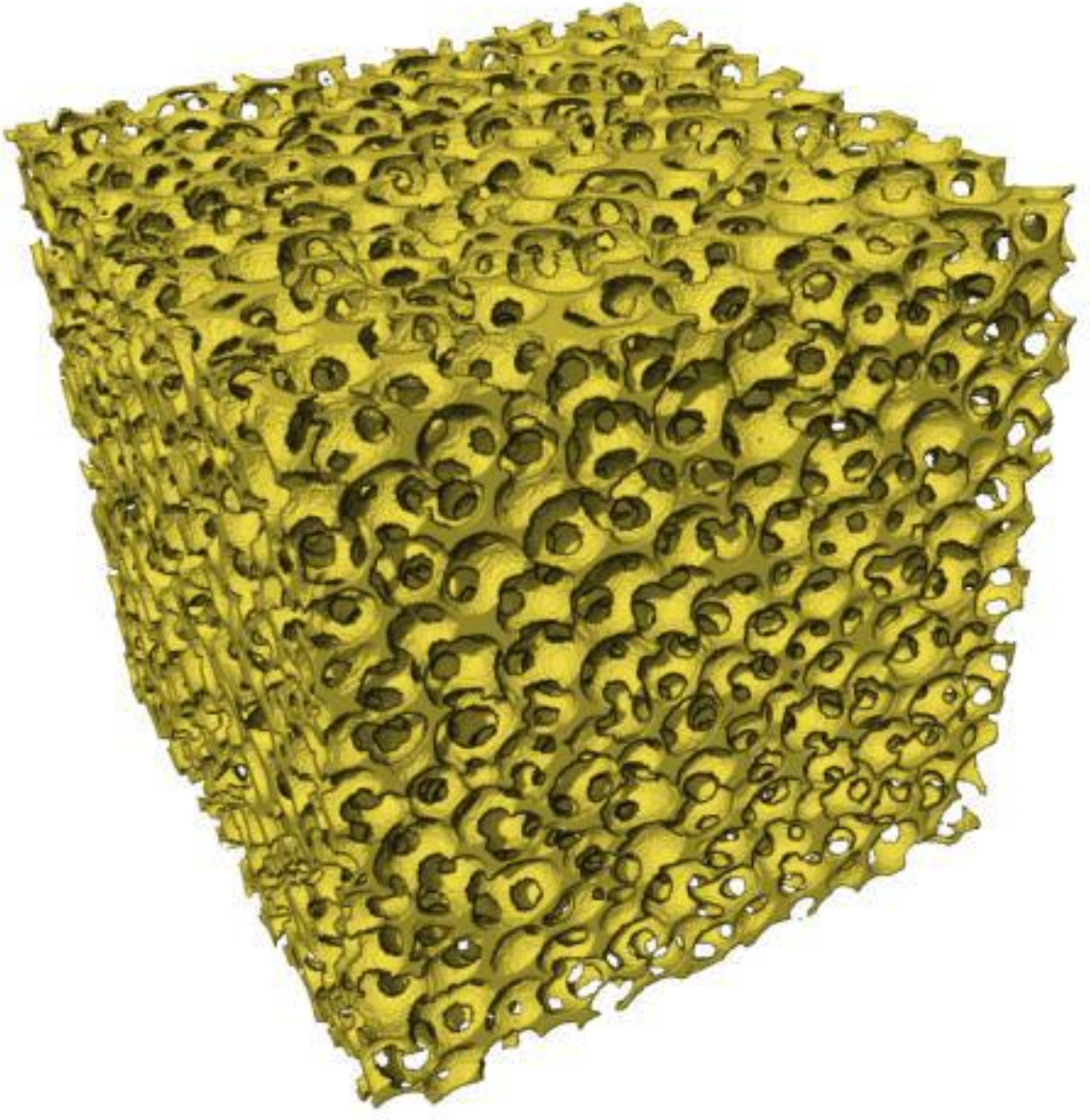

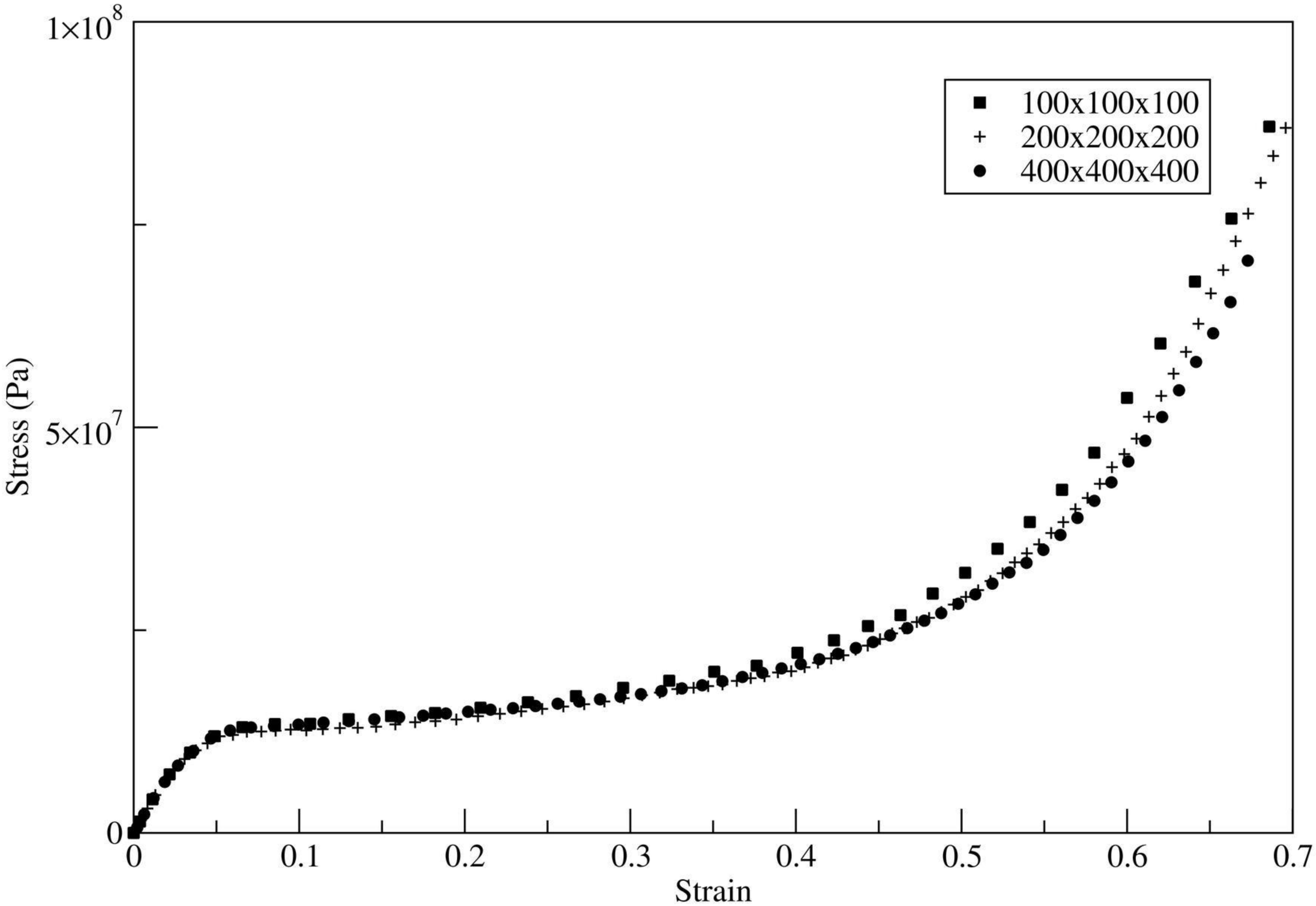
1×10^8
5×10^7
0
Stress (Pa)
0
0.1
0.2
0.3
0.4
0.5
0.6
0.7
Strain
100x100x100
200x200x200
400x400x400

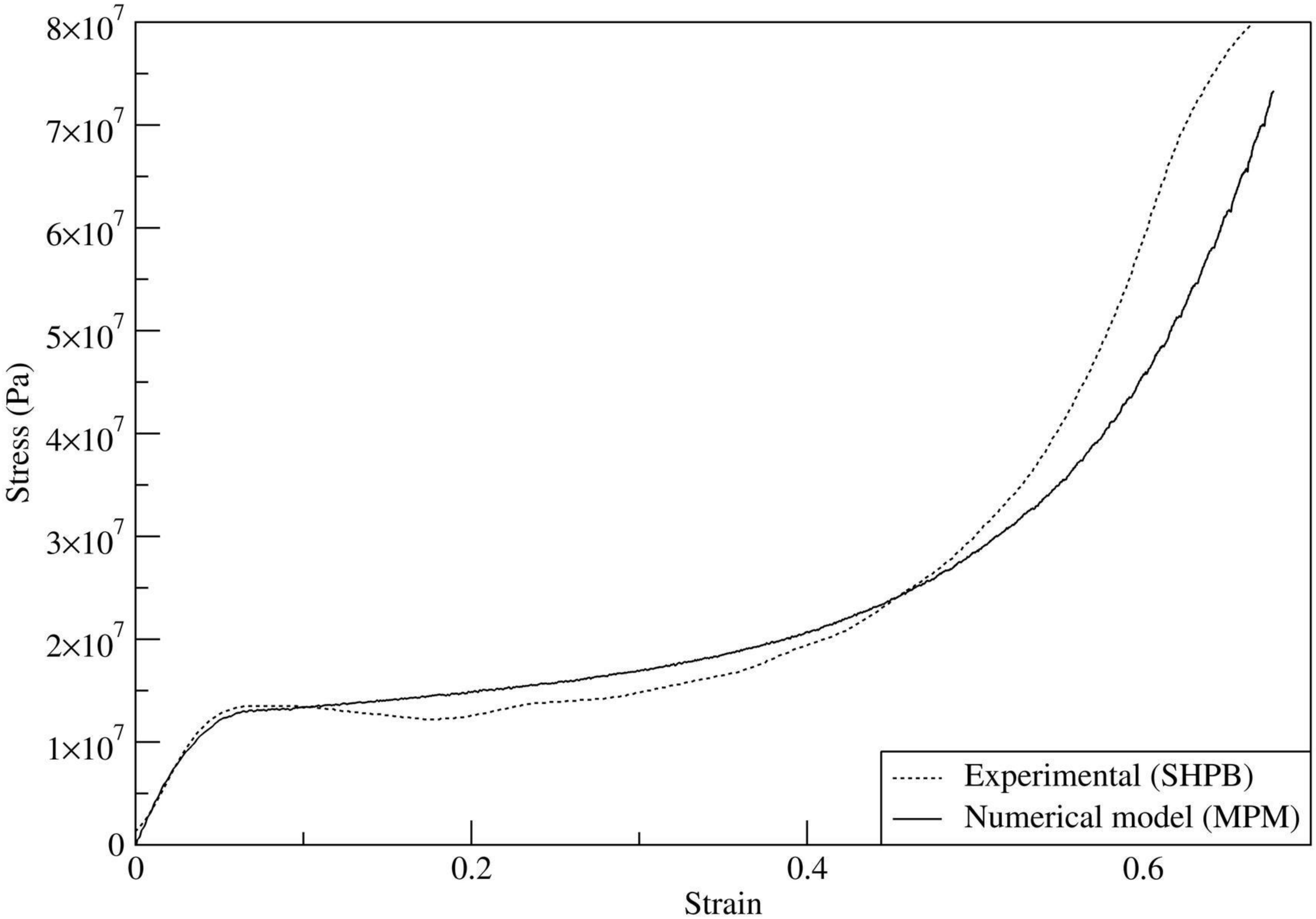
8×10^7
7×10^7
6×10^7
5×10^7
4×10^7
3×10^7
2×10^7
1×10^7
0
Stress (Pa)
0
0.2
0.4
0.6
Strain
Experimental (SHPB)
Numerical model (MPM)

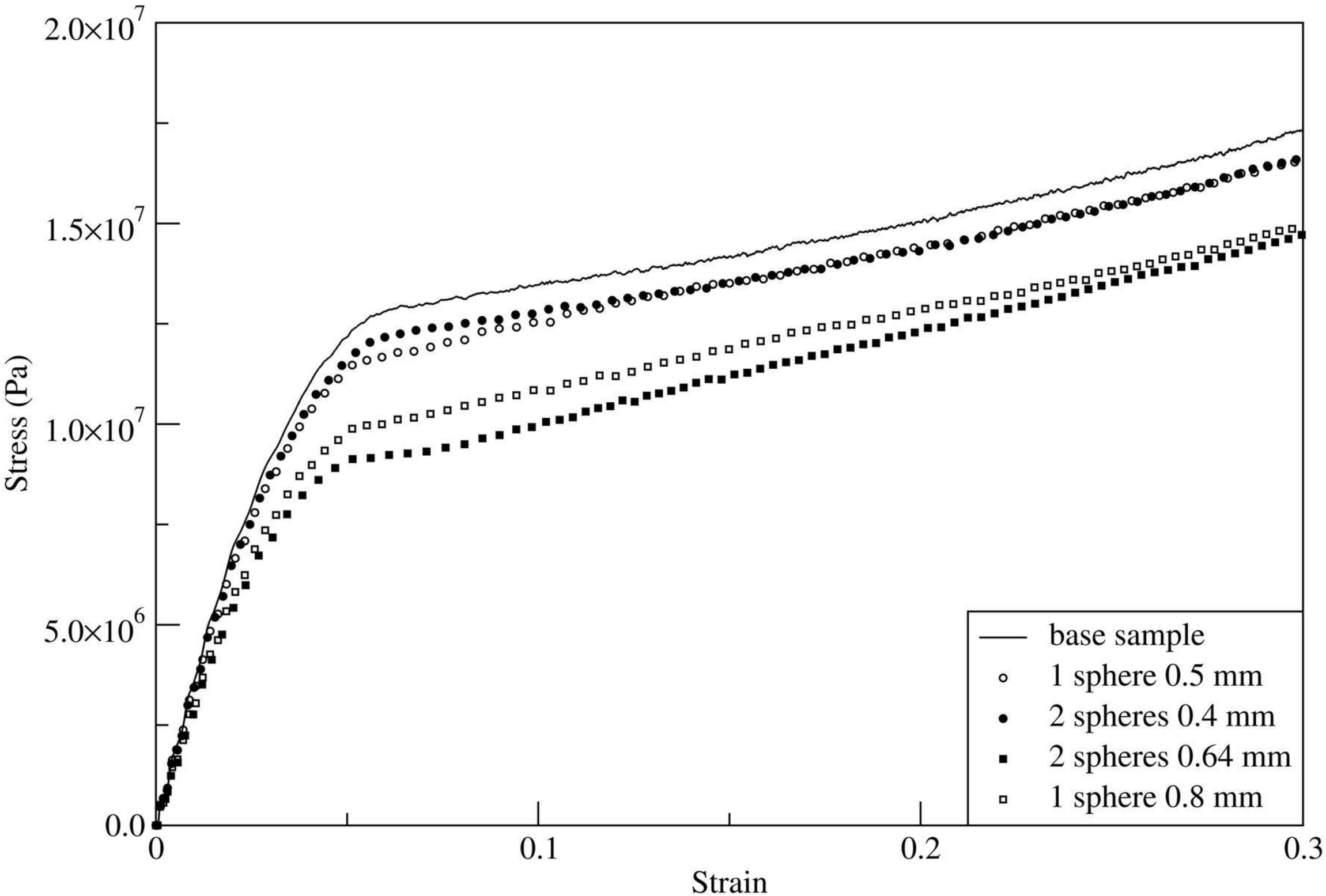
2.0×10^7
1.5×10^7
1.0×10^7
5.0×10^6
0.0
Stress (Pa)
0
0.1
0.2
0.3
Strain
base sample
1 sphere 0.5 mm
2 spheres 0.4 mm
2 spheres 0.64 mm
1 sphere 0.8 mm

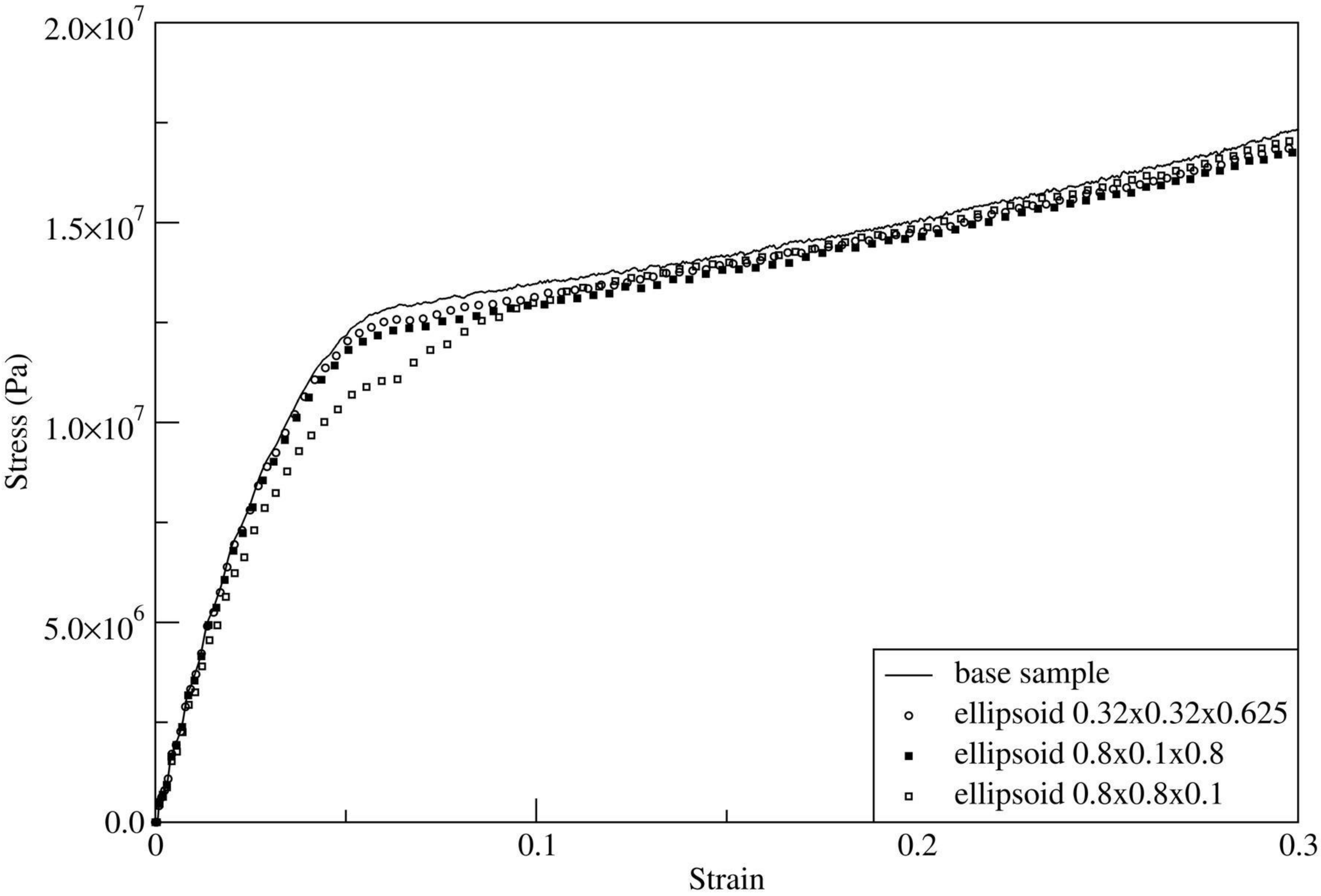
2.0×10^7
1.5×10^7
1.0×10^7
5.0×10^6
0.0
Stress (Pa)
0
0.1
0.2
0.3
Strain
base sample
ellipsoid 0.32x0.32x0.625
ellipsoid 0.8x0.1x0.8
ellipsoid 0.8x0.8x0.1

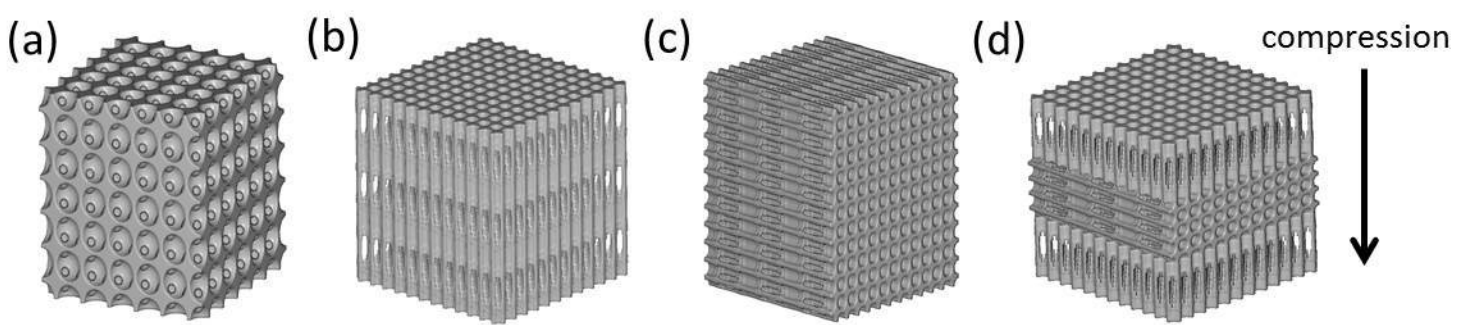
(a)
(b)
(c)
(d)
compression

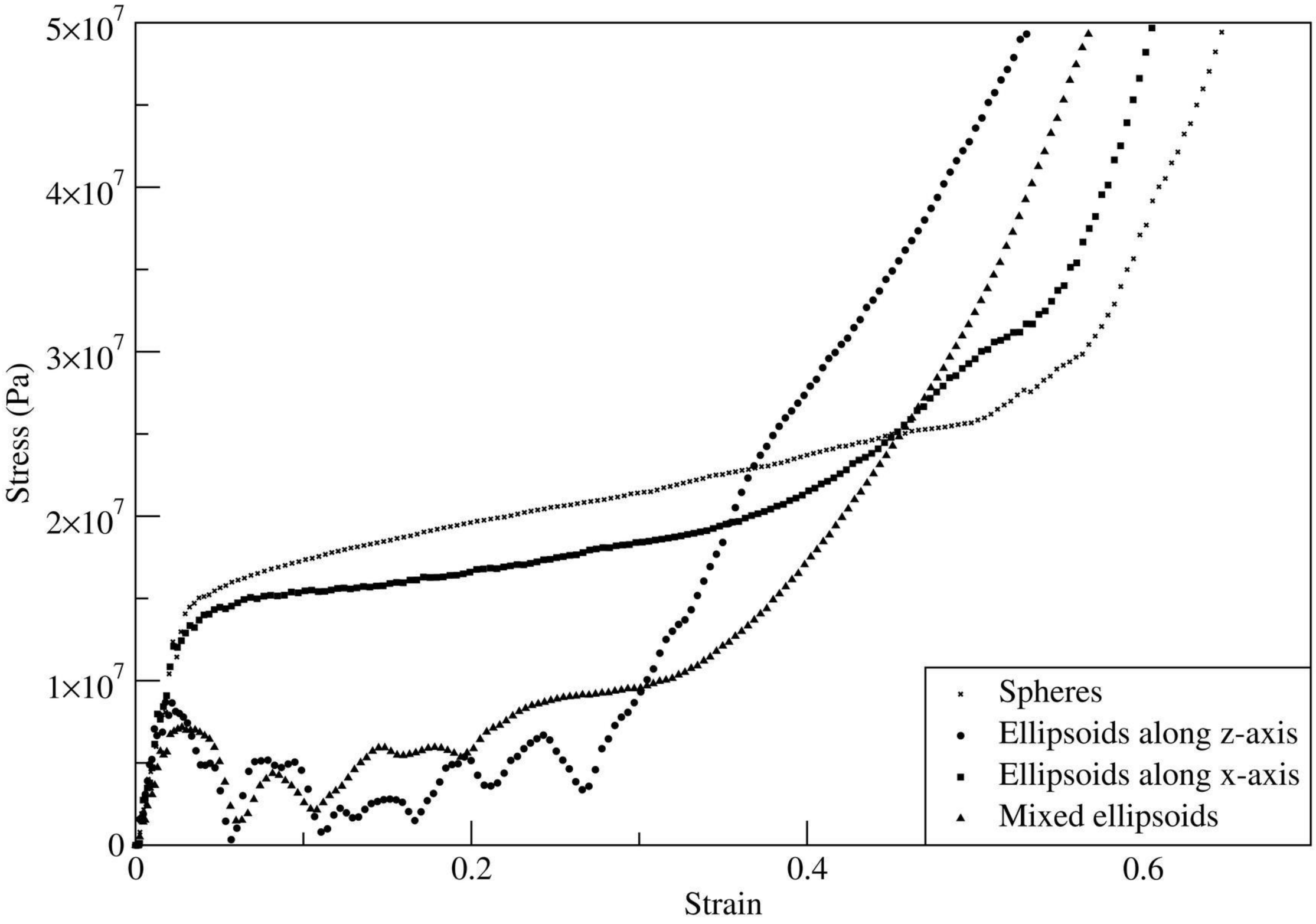
5×10^7
4×10^7
3×10^7
2×10^7
1×10^7
0
Stress (Pa)
0
0.2
0.4
0.6
Strain
Spheres
Ellipsoids along z-axis
Ellipsoids along x-axis
Mixed ellipsoids

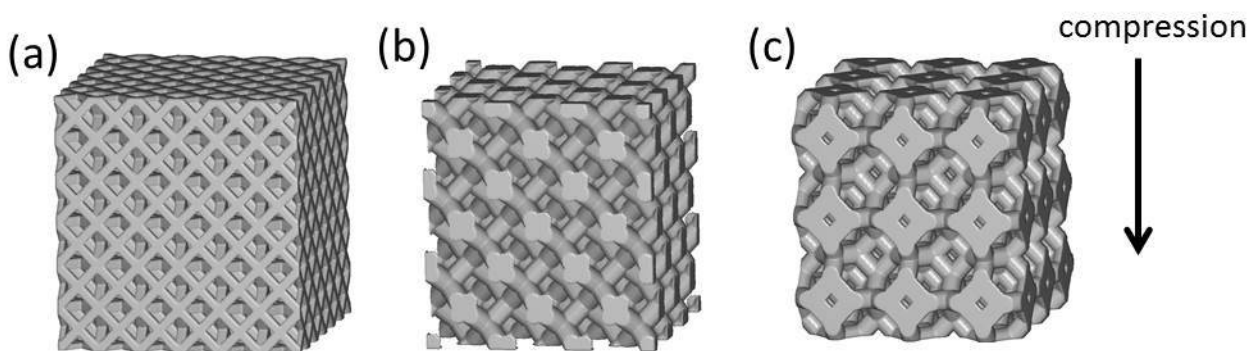
(a)
(b)
(c)
compression

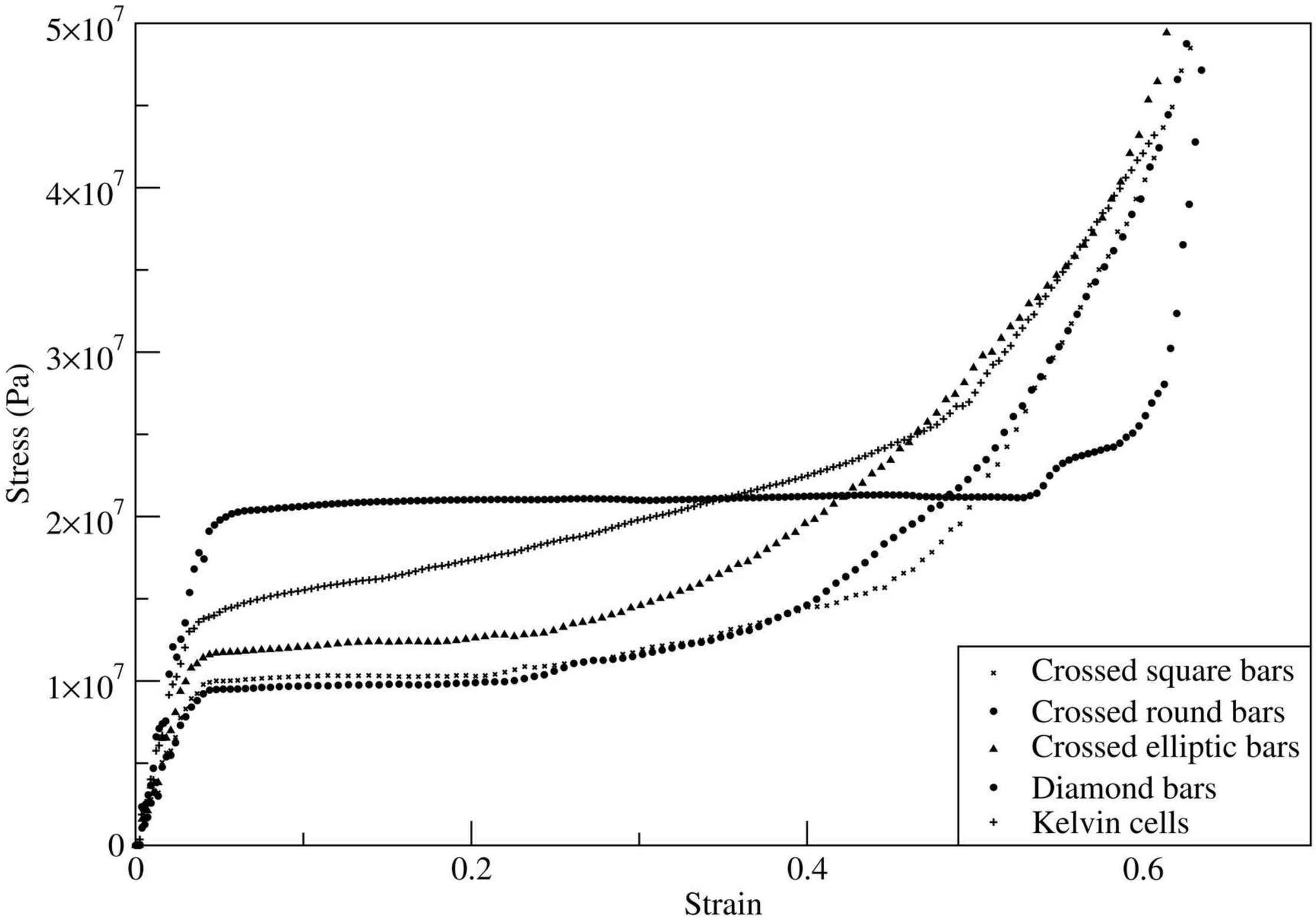
5×10^7
4×10^7
3×10^7
2×10^7
1×10^7
0
Stress (Pa)
0
0.2
0.4
0.6
Strain
Crossed square bars
Crossed round bars
Crossed elliptic bars
Diamond bars
Kelvin cells